Synthesis, Recycling and High-Throughput Reprocessing of Phase-Separated Vitrimer-Thermoplastic Blends

Liliana Miriam Aurelia Joosten, Philippe Cassagnau, Eric Drockenmuller, Damien Montarnal

Full Paper

Synthesis, Recycling and High-throughput Reprocessing of Phase-separated Vitrimer-Thermoplastic Blends

Liliana M. A. Joosten, Philippe Cassagnau, Eric Drockenmuller, and Damien Montarnal**

L. M. A. Joosten, Prof. P. Cassagnau, Prof. E. Drockenmuller

Univ Lyon, Université Lyon 1, CNRS, Ingénierie des Matériaux Polymères, UMR 5223, F-69003, Lyon, France

E-mail: eric.drockenmuller@univ-lyon1.fr

L. M. A. Joosten, Dr. D. Montarnal

Univ Lyon, CPE Lyon, CNRS, Catalyse, Polymérisation, Procédés et Matériaux, UMR 5128, F-69003, Lyon, France

E-mail: damien.montarnal@univ-lyon1.fr

Abstract. Phase-separated polymer blends including a transesterification vitrimer and polypropylene are synthesized from widely available precursors through reactive processing. We show that proper formulation during the process including a viscosity modifier of the vitrimer precursors and a reactive interface compatibilizer yields well-dispersed vitrimer phases with fractions up to 75 wt% in the polypropylene phase. These vitrimer blends can be easily reprocessed by multiple shredding-injection cycles and processed in high shear conditions through capillary rheometry. Rheological analyses reveal that a percolating dynamic network is formed across the vitrimer domains. It breaks apart during high shear reprocessing of the material and dynamically reforms after thermal annealing of the blends. It therefore ideally combines the mechanical and high-throughput (re)processing properties of the thermoplastic matrix minor phase with the chemical, thermomechanical and dynamic properties of the vitrimer major phase. This work illustrates the decoupling of processing at high shear rates enabled by the polypropylene processing aid from the kinetics of dynamic exchanges of the vitrimer phase and thermomechanical properties at service temperature of the blends.

1. Introduction

Thermosetting polymers are widely used in high-performance applications.[1] While polymer networks display outstanding performances such as enhanced chemical stability and dimensional stability at high temperatures or under loads, their recyclability is inherently limited to cost- and energy-intensive processes that are often undesirable in terms of sustainability.[2] Covalent adaptable networks (CANs) aim at overcoming these issues by integrating dynamic covalent cross-links with exchange reactions activated by triggers such as temperature or light.[3] Numerous developments have been recently reported on diverse covalent exchange chemistries involving either dissociative mechanisms (*i.e.* featuring sequential or simultaneous scission and reformation of cross-links) and associative mechanisms (also referred to as vitrimers, where dynamic exchanges occur while maintaining the network connectivity, *i.e.* constant cross-link density).[4–9] In both cases the bond reshuffling enables stress relaxation and allows the material to be reshaped under slow or limited deformations. In this regard, maintaining a low Weissenberg number (W_i is the product of the relaxation time of the material with the applied deformation rate) appears critical to avoid stress build up and fracture in the material.[10,11] In particular for vitrimers, the reprocessing is mostly carried-out by grinding and compression moulding that may involve transitory fracture, followed by multiple processes such as local relaxation, interfacial sintering and porosity decrease occurring at essentially zero shear rate.[12,13] Correspondingly, the reprocessing is directly governed by the exchange rate of the dynamic exchange reactions.[7] While the study of non-linear rheological properties of vitrimers has recently gained interest both from experimental and theoretical standpoints, flow at high shear rates is impossible for most highly cross-linked vitrimers and practically results in melt fracture or in the formation of crumbs.[14–16] Several groups have achieved regular extrusion of vitrimers by incorporating a small amount of dynamic cross-links into linear polymers such as polyolefins.[17–19] Another successful strategy is the combination of slow processing speeds with the design of vitrimers with very fast exchange dynamics.[20,21] For instance, Du Prez and coworkers designed vinylogous urethane-based vitrimers with extremely fast dynamics (relaxation time at 160 °C < 1 s), and managed to extrude at 150 °C smooth filaments using a double-twinscrew miniextruder at a speed of 1 rpm.[20] In all cases, the vitrimers had to be designed specifically to cope with the process: low cross-link density or low gel fraction, very fast exchange reactions induced by high amounts of catalysts or combination of dual dynamic bonds in series. Such workarounds unfortunately weaken the creep resistance of the vitrimers at service temperature. An alternative approach was recently proposed by Guo and co-workers.[22] They found that curing a styrene-butadiene rubber (SBR) in the presence of 10 phr of dithiol cross-linker containing dynamic dioxaborolane linkages leads to difficult processing: vane

extrusion of this highly cross-linked dynamic rubber (100 rpm, 190 °C) essentially lead to fractured crumbs. However, after grinding the material into micron-sized powder, and blending it with an SBR containing 2 phr of dynamic cross-linker, the resulting material was processable by vane extrusion. This behavior is most likely related to the appropriate design of a two-phase blend with: i) comparable chemical nature of the polymer backbone and dynamic cross-linker affording ideal interfacial adhesion, and ii) highly cross-linked dispersed phase acting as reinforcement of the loosely cross-linked dynamic matrix enabling processability.

Dispersion of highly cross-linked elastomers in thermoplastics by in-situ crosslinking during blending is in fact amongst the few successful strategies that have led to the industrial development of (re)processable permanent elastomers. These materials called thermoplastic vulcanizates (TPVs) have historically been obtained from the dispersion of a high volume fraction (>60 vol. %) of a cross-linked EPDM rubber in a polypropylene matrix, and subsequently extended to a larger variety of materials (*e.g.* polyamide matrixes, silicone rubbers).[23] The desired objective is to combine the elasticity of the cross-linked rubber phase (*e.g*. low modulus, high creep resistance and elasticity recovery) with the melt processability in high-shear conventional devices (extruders, internal mixers, injection press) of the thermoplastic matrix. Blends such as TPVs are produced *via* a single reactive processing step, where the elastomer phase is selectively cross-linked during high-shear blending with a thermoplastic. In such blends, the mechanical performance is governed by the final morphology and the particle size. During processing, the blend morphology typically evolves from thermoplastic droplets dispersed in the un-cross-linked elastomer matrix to cross-linked elastomer particles dispersed in the thermoplastic matrix following a phase-inversion process.[24–29] In the melt, attractive interactions across elastomer particles form a physical network, and the blend behaves as a yield stress fluid.[30] At service temperature, the crystallinity of the thermoplastic matrix dramatically increases the yield stress and the resulting materials demonstrate elastomer properties.

The present work applies the concept of TPVs to vitrimer-based materials and proposes a versatile strategy that enables high shear rate processing methods while mitigating the lower mechanical performance typical of highly cross-linked vitrimers (*i.e.* low strength and strain at break). It consists in a reactive blending strategy that converts commercially available low-cost vitrimer precursors and a molten thermoplastic into a fully cured phase-separated blend using a straightforward and up-scalable single-step process. It affords in relatively short reaction times a fine dispersion of cured vitrimer particles in a PP matrix. Extensive structural and rheological characterizations of blends involving 12-75 wt% vitrimer phase (**S_{12}-S_{75}**) are carried out and compared to the pure vitrimer (**S_{100}**) and PP (**S_0**) reference

materials. For the first time in the field of CANs, capillary rheology has been implemented in order to measure viscosities at high shear rates and demonstrate in particular that the viscosity of the blends can be decoupled from the bond-exchange dynamics.

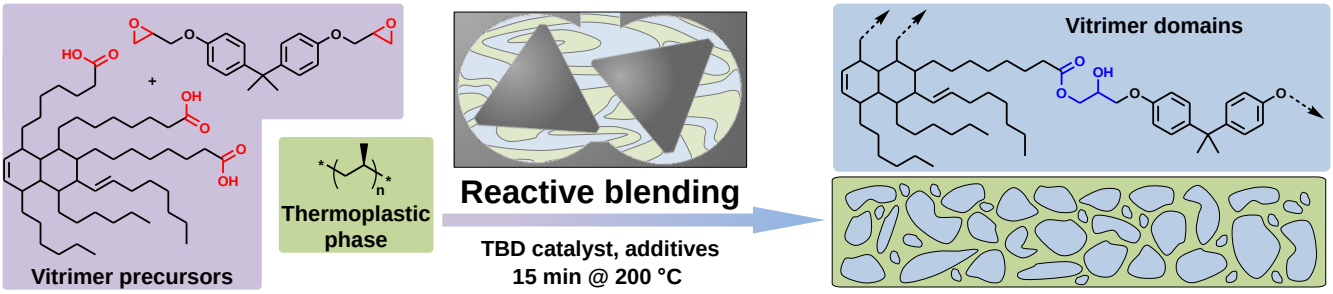

Figure 1. Reactive blending strategy between a thermoplastic phase (PP) and an epoxy-acid vitrimer phase.

2. Results and Discussion

2.1. Reactive processing of PP/vitrimer blends

Up-scalable formulations involving inexpensive and largely available commercial precursors were selected to demonstrate the reactive blending of vitrimer precursors and a thermoplastic phase (**Figure 1**). A standard injection grade PP was chosen as the thermoplastic matrix. The vitrimer phase, relying on associative transesterification covalent exchanges, was obtained from the curing of di/trimerized fatty acids (Pripol 1040) and an aromatic diepoxy (DGEBA) in the presence of 1,5,7-triazabicyclo[4.4.0]dec-5-ene (TBD) to catalyze both network formation and subsequent transesterification exchanges. This classic vitrimer formulation is particularly robust and stable at high temperatures.[31] It has been widely studied, extended to various catalysts and epoxy/acid building blocks such as bio-based precursors and applied to different fields such as composites, 3D-printing of closed-loop recyclable materials or recyclable super-amphiphilic membranes for water filtration.[32–39] While this particular system is relatively brittle and displays rather slow exchanges kinetics, it is a very relevant candidate to decouple (re)processing timescales and network-relaxation timescales. TBD was chosen as catalyst, as it is soluble in Pripol at elevated temperature, thereby facilitating its homogeneous dispersion and catalytic activity during reactive processing. Curing kinetics at 200 °C of the pure vitrimer were studied by rheology: using 5 mol% of TBD with respect to COOH/epoxy groups, the gel point was reached within 80 s which is commensurate with high-throughput processing in an extruder and complete curing was obtained within 300 s (Figure S1, Supporting Information). The complete curing of the vitrimer was corroborated by

time-resolved FTIR monitoring at 200 °C (Figure S2, Supporting Information). The disappearance of carboxylic acid and epoxy bands (at 1710 and 912 cm^{-1}, respectively), and the concomitant increase of the ester band (at 1735 cm^{-1}) can also be observed within 400 s. Accordingly, the processing temperature was fixed at 200 °C and the processing time after adding all reagents in the melt mixer was maintained at 10 min throughout the study.

Reactive processing of a 12:88 (wt/wt) vitrimer/PP blend was initially carried out using a melt mixer by sequential addition of PP, Pripol/TBD mixture and DGEBA. The temperature and torque are recorded throughout the process, and the addition steps are visible in the profiles (Figure S3, Supporting Information). The sharp increase of the torque after 15 min corresponds to the increase in viscosity caused by the cross-linking reaction of the vitrimer phase after addition of DGEBA. To prevent thermal degradation of PP chains, a commercial antioxidant (0.5 wt% Irganox 1010) was added to the thermoplastic phase. HT-SEC confirmed that after melt blending PP with Irganox 1010 for 30 min at 200 °C, the decrease in number average molar mass of PP is negligible (Table S1, Supporting Information). Optical microscopy of the resulting blend demonstrates the presence of macroscopic vitrimer domains (median size of 0.6 mm) dispersed in the PP major phase (Figure S4a, Supporting Information). Two distinct strategies were then examined independently in order to improve this relatively poor mixing efficiency. First, PP grafted with maleic anhydride (PP-*g*-MA) was chosen as reactive interface compatibilizer. The grafted maleic anhydrides can indeed react with epoxides or alcohols in the vitrimer phase to form copolymers that reduce the surface tension between the vitrimer and PP phases. This strategy is well known to improve dispersion during reactive blending and eventually obtain nanophase structuration.[40] Herein, addition of PP-*g*-MA (10 wt% with respect to PP) during the processing results in a moderate decrease of particle sizes (median of 0.25 mm) compared to the blend without additives (Figure S4b, Supporting Information). In a second strategy, we aimed at reducing the viscosity mismatch between molten PP and vitrimer precursors. Droplet breakup when blending two immiscible liquids is indeed known to be primarily determined by the dimensionless viscosity ratio λ:[41]

$$\lambda = \frac{\eta_d}{\eta_m} \quad (1)$$

where η_d is the viscosity of the dispersed phase and η_m the viscosity of the matrix (λ is initially about 10^{-5} for the Pripol/PP mixture at 200 °C). In pure shear flow, which is the predominant mode in internal mixers, the breaking of droplets is most efficient for $0.1 < \lambda < 1$ and decreases dramatically when $\lambda < 10^{-2}$.[42] Mixing efficiency may also be further decreased because we are mixing a Newtonian liquid (Pripol, then DGEBA) into a viscoelastic fluid.[43] While the viscosity of the vitrimer phase is expected to rise sharply during curing, the effective time-window for efficient mixing ($\lambda > 10^{-2}$) before gelation

occurs is extremely narrow (typically starting about 50 s after addition of DGEBA and lasting about 30 s). Our strategy aimed thus at adding inorganic fillers to increase the initial viscosity of the Pripol phase and benefit from an extended time-window for efficient mixing (typically 5 min of Pripol/PP mixing before addition of DGEBA).[44] A hydrophilic fumed silica (Aerosil 200 from Evonik) was dispersed in Pripol (15 wt% according to Pripol) using a planetary mixer until full transparency is reached. Curing kinetics at 200 °C of a pure vitrimer phase using Pripol/A200$_{15\%}$, DGEBA and TBD confirmed that adjunction of silica does not change the gelation time (Figure S1, Supporting Information). However, the final modulus and the T_g attained are slightly higher in presence of silica (1.63 *vs* 1.27 MPa, and 15 *vs* 12 °C with and without silica, respectively) and, more importantly, the similar values of *G*' and *G*'' before gelation indicate a more complex viscoelastic behavior. Additional characterization at 200 °C of the Pripol/A200$_{15\%}$ mixture in absence of DGEBA indicates a viscoplastic behavior, with static and dynamic yield stresses about 140 Pa and 80 Pa, respectively (Figure S5, Supporting Information). When comparing to pure Pripol, the corresponding viscosities are increased by a factor up to 10^4 at 1 s^{-1}. Such improvement in the viscosity ratio of dispersed and matrix phases ($\lambda \sim 10^{-1}$ at 200 °C) resulted indeed in a drastic improvement of the mixing efficiency between the vitrimer and PP immiscible phases, with median sizes of the vitrimer domains decreasing to 10 μm (Figure S4c, Supporting Information). Finally, the two strategies above were combined to carry out the reactive processing of all vitrimer/PP blends studied herein: **i)** addition of PP + 10 wt% PP-*g*-MA + 0.5 wt% Irganox 1010 in the melt mixer preheated at 200 °C, **ii)** after the torque has stabilized (about 5 min), addition of Pripol mixture in which 15wt% A200 silica and TBD catalyst were pre-dispersed, **iii)** after 5 min, addition of DGEBA, and **iv)** after 10 min of curing, recovery of the material and hot-pressing into 1.5 mm thick sheets. The fully formulated 12:88 vitrimer/PP blend comprised vitrimer domains with median sizes of 0.8 μm, and results in fully homogeneous sheets at the optical scale (Figure S4d, Supporting Information). The concept was further extended by varying the vitrimer:PP ratios from 12 to 75 wt.% vitrimer, referred to as **S$_{12}$** to **S$_{75}$** in the following. The **S$_0$** (PP:Irganox) and **S$_{100}$** (vitrimer:silica obtained by curing the liquid vitrimer precursors in the press) are added as references (Figure S6, supplementary information). The detailed compositions of all samples are given in Table S4, Supporting Information. Significant curing of the vitrimer phase after the procedure steps was confirmed by FTIR (Figure S7, Supporting Information), demonstrating low amounts of residual carboxylic acids (typically <25%) and total disappearance of epoxy bands. The bulk morphology of blends **S$_{12}$-S$_{75}$** (**Figure 2**) shows silica aggregates essentially localized in vitrimer domains (Figure S8, supplementary information), as anticipated from the higher polarity of the vitrimer phase than the PP phase and from the initial dispersion of silica in Pripol.

While vitrimer domains appear well-dispersed into a "sea-island" morphology for low fractions (**S_{12}** and **S_{24}**), a bimodal distribution appears for higher vitrimer loadings, with submicronic domains but also larger and more complex shaped domains due to droplet coalescence or less effective mixing during the synthesis. This results in elongated shapes as the shear-deformed vitrimer droplets are cross-linked by the fast curing reaction. For **S_{48}**, **S_{60}** and **S_{75}** the delimitation between particles and matrix becomes ambiguous, typical of morphologies near co-continuity.[45]

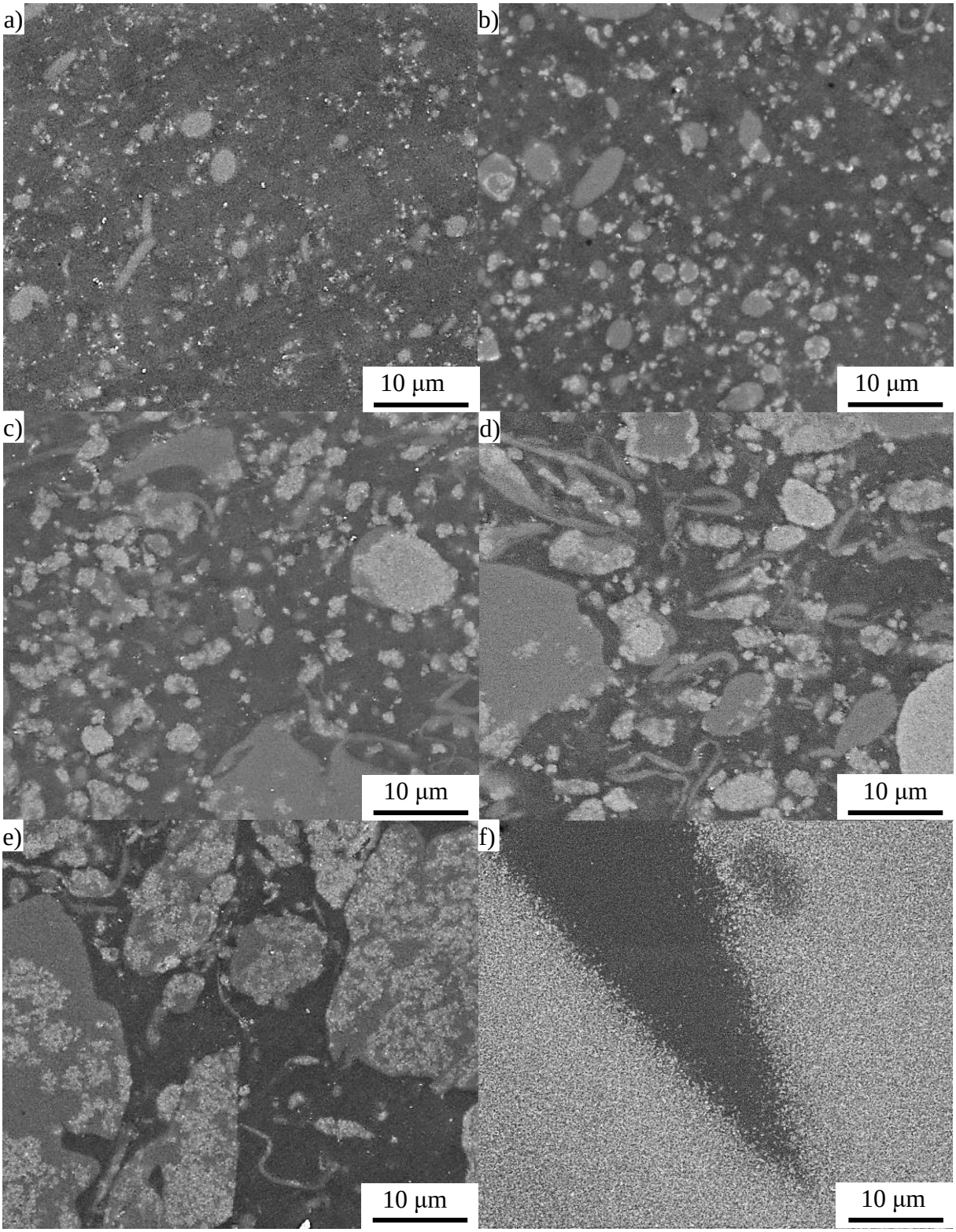

Figure 2. SEM of vitrimer blends after surfacing by cryo-microtomy. a) $\mathbf{S_{12}}$; b) $\mathbf{S_{24}}$; c) $\mathbf{S_{48}}$; d) $\mathbf{S_{60}}$; e) $\mathbf{S_{75}}$ and f) $\mathbf{S_{100}}$. SEM-EDX analysis (Figure S8, supplementary information) enabled to readily assign the

different phases of the observed morphologies, *i.e.* PP in dark grey, vitrimer in light gray and silica aggregates in white.

2.2. Thermo-mechanical study

Table 1. Physical and rheological properties.

Sample name	Vitrimer content [wt%]	$E'_{100°C}$ [a)] [MPa]	$E'_{200°C}$ [a)] [MPa]	G_N [b)] [kPa]	τ^* [b)] [s]	Gel fraction [c)]	Swelling ratio [c)]
S_0	0	520	/	/	/	/	/
S_{12}	12	590	/	/	/	/	/
S_{24}	24	440	/	0.8	1930	0.96	4.5
S_{48}	48	220	0.45	18	2650	0.99	3.8
S_{60}	60	170	0.45	72	1700	0.98	2.99
S_{75}	75	120	1.1	130	2030	0.97	2.22
S_{100}	100	6.3	8.1	540	3400	0.93	1.55

[a)]measured with DMA; [b)]network moduli and relaxation time calculated from fitting the stress relaxation performed at 200 °C to a stretched exponential decay function (see Characterization Methods); [c)]determined after 48h in xylene at 110 °C, normalized to the weight fraction of the vitrimer phase and PP-*g*-MA.

The blends **S_{12}** to **S_{75}** show a good thermal stability, with a temperature at 5% weight loss in the 380-400 °C range independent of the vitrimer content (Figure S9, Supplementary Information) and ash residuals proportional to the amount of silica in each blend. DSC thermograms reveal that vitrimer domains barely impact the melting temperature of the PP phase (Table S2 and Figure S10, Supporting Information). The T_g of the vitrimer phase is noticeable for high vitrimer fractions around 15-20 °C. The crystallinity measured from the melting enthalpy and normalized by the PP fraction is constant about 45 %. Distinctions between samples can however be found during crystallization: whereas pure PP displays two separate crystallization exotherms at 113 °C and 123 °C, which are commonly attributed to a highly ordered and a less ordered α-phase, vitrimer blends show a single crystallization exotherm at 121-127 °C, characteristic of a nucleating effect resulting from the presence of small and well dispersed vitrimer domains.[46–48] This is interestingly corroborated by DSC characterization of **S_{60}** that does not contain silica and/or PP-*g*-MA additives – therefore comprised of very large vitrimer domains - and that

does not exhibit such nucleating effect (Figure S11, Supporting Information). Further analysis of the crystalline structure by wide angle x-ray diffraction (WAXD, Figure S12, Supporting Information) reveals the predominance of the α-phase in the PP crystallites. However, **S12** and to a lesser extent **S24** show an additional *β*-phase evidenced by a diffraction peak at 2θ = 16.2°. Similar *β*-nucleation effects have been previously reported for highly dispersed vulcanizate particles in PP/EPDM TPVs.[49,50] Small angle x-ray scattering (SAXS) at room temperature revealed for the pure PP distinctive scattering of a lamellar structure (q_0 = 0.045 Å^{-1} after Lorentz correction; Figure S13a, Supporting Information). The correlation function analysis using the SasView software yields the typical profile expected for a semicrystalline arrangement, with a long period L_p = 13 nm and a narrow interface thickness of *ca.* 0.5 nm. Upon inclusion of 10% PP-*g*-MA and progressive increase of the vitrimer fraction, the scattering signal due to the lamellar structure of PP indicates first an increase of the long period and then becomes less and less visible in comparison to the strong scattering of silica aggregates in the vitrimer domains. Kratky analysis (scattering signal around q = 0.01 Å^{-1}) gives an estimation of silica aggregate sizes constant about 60 nm (Figure S13b, Supporting Information). The strong up-turn of the scattering intensities at low q-values for blends but not for **S100** and **S0** also indicates phase separation into domains with sizes well above 100 nm, consistently with the morphologies observed by SEM (Figure S4, Supplementary Information).

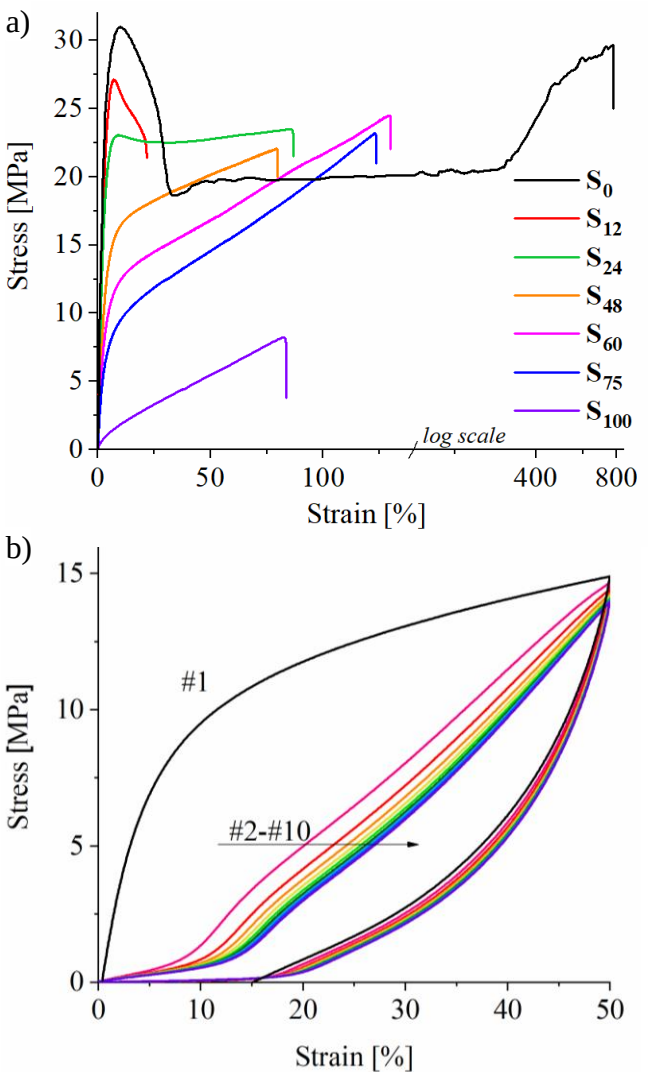

Figure 3. a) Tensile testing (10 mm min^{-1}) of vitrimer/PP structured blends, PP and the pure vitrimer; b) Cyclic testing showing hysteresis curves up to 10 cycles for prestrained **S$_{60}$** sample. Experiments performed near 20 °C.

Tensile tests are relatively sensitive to the testing temperature given the T_g of vitrimer phases around 15 °C. Tests have thus been run near 20 °C using slow deformation speeds (10 mm min^{-1}) to minimize the typically expected stress softening profiles. The results show nevertheless a large range of behaviors depending on the sample composition (**Figure 3a**; Table S3, Supporting Information). PP shows the classical rigid and ductile behavior of a thermoplastic, including high modulus, yield point around ε = 20% and strain hardening at ε > 300%. The pure vitrimer presents a relatively high Young's modulus typical of a filled elastomer (E = 9 MPa) and a brittle elastic behavior (ε_{max} = 80%). **S$_{12}$** and **S$_{24}$** evidence thermoplastic behaviors close to PP by large moduli and yield points, but highly reduced elongation at

break. The behavior of the vitrimer phase is dominating for **S$_{48}$**, **S$_{60}$** and **S$_{75}$**, with an initial rigidity however dictated by the PP fraction. Interestingly, both stress and strain at break are significantly increased in the blends compared to the rather brittle **S$_{100}$** vitrimer reference. Pre-stretching the samples **S$_{60}$** and **S$_{75}$** at 50% strain (*i.e.* beyond the yield point of **S$_0$**) is almost fully recoverable and results in softer materials comparable to highly filled elastomers, with moduli about 23 and 17 MPa, respectively (Figure S14**a**, Supporting Information). We confirmed the elastic recovery at 50% strain of sample **S$_{60}$** by performing cyclic tensile testing (**Figure 3b** and Figure S14b, Supporting Information). The corresponding elastic recovery above 90% after 10 stretch cycles indicates an excellent dimensional stability and supports the formation of a percolating network across vitrimer domains. The influence of phase dispersion on the tensile properties is illustrated in Figure S15b, Supporting Information. In absence of silica (following previously described recipes), the **S$_{60}$** blend shows poor properties (ε_{max} = 70%), and almost immediate failure (ε_{max} = 10%) in absence of compatibilizers. Other studies on vitrimer nanocomposites, reinforced with precipitated silica, graphene or carbon nanotubes, also found that the addition of nanofillers increases the moduli at the expense of decreasing the elongation at break.[51–53] The good mechanical performances in the sample containing both silica and compatibilizer in our case can be attributed to a finer morphology (See Figure S15c-f, Supporting Information), an effect already well-known in the case of conventional TPVs.[49] This result also emphasizes the importance of forming adequate interactions across vitrimer domains to control the mechanical properties of the blends, and the possible role of PP-*g*-MA in this regard.

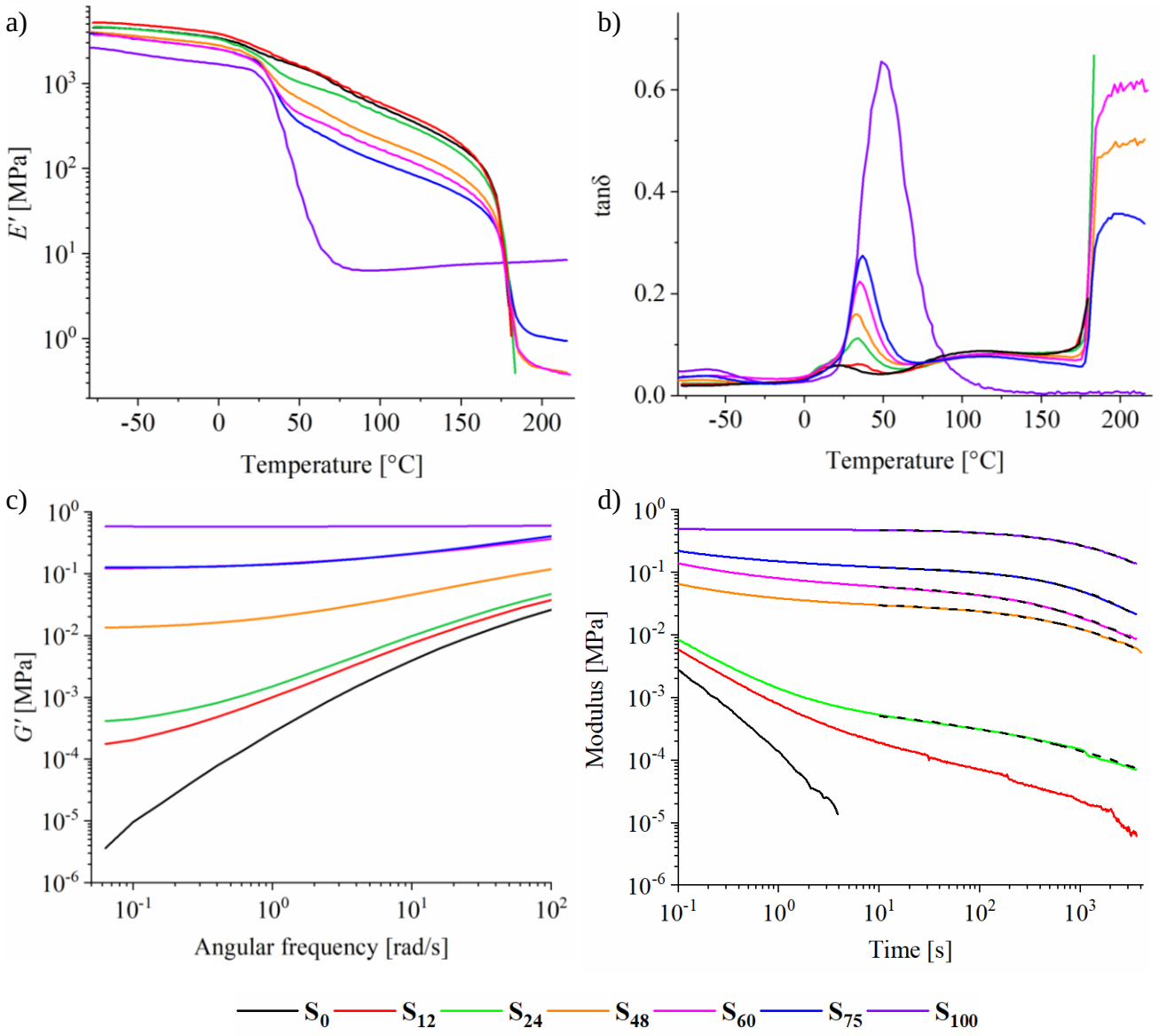

Figure 4. Thermo-mechanical characterization of **S0-S100**. a,b) Temperature ramp measured by DMA (3 °C min^{-1}, 1 Hz), showing the traces of storage modulus (*E*'), and tan(δ). Characterization by rotational rheology: c) SAOS at 200 °C (1% strain, the loss moduli are omitted for clarity), and d) stress relaxation at 200 °C (1% strain). Data were fitted using a stretched exponential decay (Equation 2; black dashed lines).

DMA analysis was performed from -80 to 220 °C to analyze the thermomechanical behavior of **S0-S100** (**Figure 4a,b**). The α-transitions for vitrimer and PP phases are partially distinguishable (Table S2, Supporting Information). While $T_{\alpha\text{-PP}}$ remains constant at 20 °C, $T_{\alpha\text{-vit}}$ is gradually increasing with the vitrimer loading from 35 to 52 °C (for **S12** and **S100**, respectively). Such evolution appears associated to

the dispersion state of the vitrimer domains and might therefore originate either from a confinement effect or, more likely, from a better compatibilization and larger PP/vitrimer interphase as the ratio of PP-*g*-MA to vitrimer is effectively considerably higher for low fractions of vitrimer. Around 53 °C, a secondary $T_{\alpha*}$ transition is visible in PP-rich blends that corresponds to a crystal-crystal slip in the PP phase (**Figure 4a**).[54] Above the melting temperature of PP (near 170 °C), the sudden drop in modulus is concomitant with failure of samples **S$_{12}$** and **S$_{24}$**. However, an elastic plateau visible in **S$_{48}$**, **S$_{60}$** and **S$_{75}$** suggests the formation of a percolating vitrimer network. Complementary linear rheology measurements were thus performed in the melt (200 °C, **Figure 4c**). For **S$_{48}$**, **S$_{60}$** and **S$_{75}$**, the elastic plateaus at low frequencies on the storage moduli confirm the presence of a network across vitrimer domains. Stress relaxation enables to probe the dynamics of the blends beyond the relaxation of PP chains and define more accurately the modulus of the percolating network (**Figure 4d**). We found in this way that networks can be obtained with vitrimer fractions as low as 24%. While a similar formation of percolating network is often encountered in TPVs or rubber-modified thermoplastics, vitrimer blends display an additional relaxation at longer timescales. We attribute this relaxation to dynamic rearrangements within the percolating vitrimer network.[26,55] The corresponding relaxation times (**Table 1**) are in the same order of magnitude (1000 to 2000 s at 200 °C), yet slight faster than that of pure vitrimer around 3400 s. Discrepancies in these values might be related to variation in the effective formation of percolating vitrimer network that depends on the thermal and processing history of the samples as discussed further afterwards. The attribution of this relaxation event to dynamic network exchanges was further confirmed by preparing **S$_{60}$** with various concentrations of TBD catalyst at 2.5, 5.0 and 10 mol% with respect to COOH/epoxy groups (Figure S16, Supporting Information). The network relaxation of the blend is indeed accelerated for higher TBD contents (*i.e.* $\tau*$ = 2250, 1700 and 750 s for 2.5, 5.0 and 10 mol% TBD, respectively).

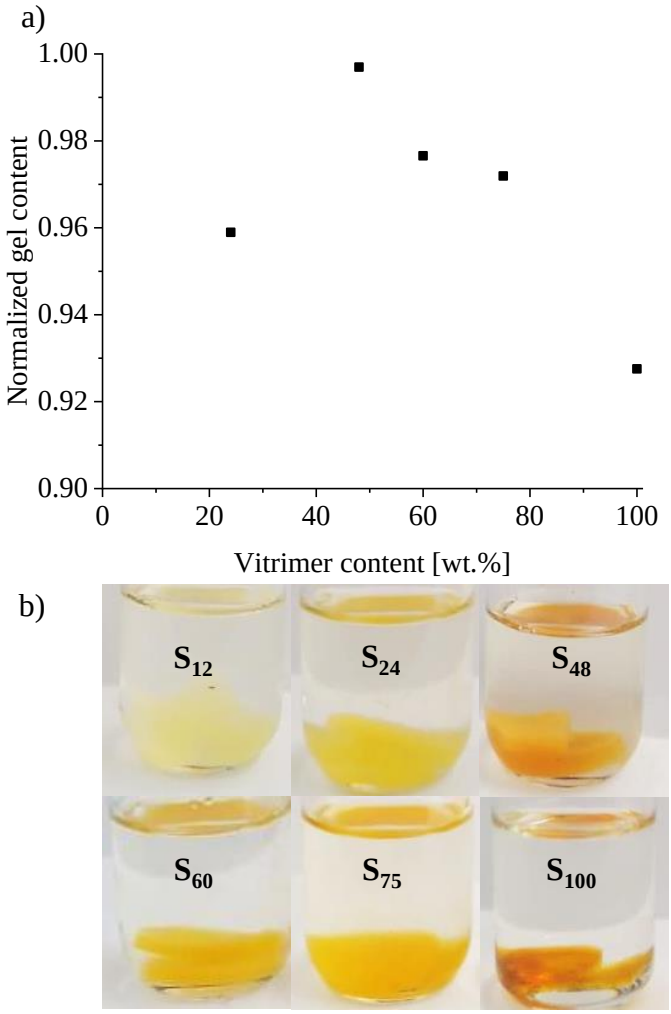

Figure 5. a) Gel fraction of PP/vitrimer blends swollen in xylene (24h at 110 °C), normalized to the initial content of vitrimer precursors and PP-*g*-MA. No measurable value was achieved for **S12**, as the sample disintegrates into particles; b) samples **S12 - S100** in their swollen state, after 48h in xylene at 110 °C.

Swelling in hot solvents, capable of dissolving the PP phase, is a particularly uncompromising test to determine co-continuity in blends, such as TPVs.[56,57] Herein, after immersion for 48 h in xylene at 110 °C, **S0** dissolves completely while **S100** shows a gel fraction of 93% and a swelling ratio of 1.7 (**Table 1**). Extraction of **S12** leads to a dispersion of swollen vitrimer particles, while all other blends retain a monolithic shape and swell homogeneously (**Figure 5**). The gel content, normalized to the vitrimer fraction and assuming that all PP-*g*-MA remains tethered to the vitrimer network, remains constant at about 0.93 – 0.99. This corroborates that mixing of vitrimer precursors and catalyst occurred homogenously in the dispersed vitrimer domains and produced fully cross-linked vitrimer domains,

where the cross-linking density is independent of the vitrimer weight fraction in the blend. The swelling ratio increases significantly for samples having lower fractions of vitrimer phase (Table 1). We believe that this "sponge effect" is ascribed to free solvent trapped within open pores formed by the network of vitrimer particles.

2.3. (re-)Processing and recyclability.

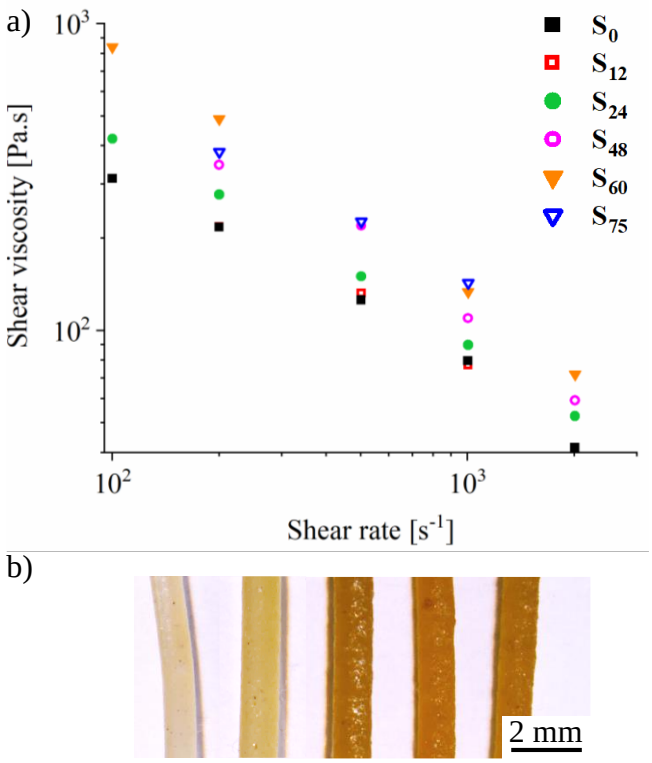

Figure 6. a) Viscosity flow curve for **S_0-S_{75}**, obtained from capillary rheometry at 200 °C; and b) resulting extrudates from left to right: **S_{12}**, **S_{24}**, **S_{48}**, **S_{60}** and **S_{75}**.

The linear rheology, structural and mechanical characterizations all point to the formation of a percolating vitrimer network with relatively slow relaxation dynamics (*ca.* 2000 s at 200 °C). In contrast, the reactive blending strategy chosen involves medium shear rates (estimated below 50 s^{-1}) and yet leads to torques well within the working range of the melt mixer, as well as easy mold-pressing over short times. The presence of the PP phase and its role as processing aid appear thus essential to enable fast melt-processing independently from the slow exchange dynamics of the vitrimer network. This also suggests that the percolating network across vitrimer domains must be partially disrupted during high shear processing. To confirm this hypothesis, several creep steps with increasing stresses ranging from

50 to 7000 Pa were performed on sample **S60**, and the corresponding viscosities were determined from the compliance (Figure S17, Supporting Information). Up to 5000 Pa, **S60** demonstrates relatively constant viscosity about 10^8 Pa s, *i.e.* in line with the result expected from linear relaxation data ($\eta = G.\tau = 1.2 \times 10^8$ Pa s) and thus characteristic of dynamic exchanges within the percolating vitrimer network. At 7000 Pa, a dramatic increase of shear rate indicates yielding into a viscous melt and breaking of the vitrimer network. Such rupture is however only partial as stopping and relaunching the creep steps experiment (2nd run) gives the same results, albeit with a lower yield stress about 3000 Pa. Capillary rheometry was then used to investigate the melt flow of the vitrimer/PP blends through a narrow die (1 mm diameter) at high shear rates ranging from 100 to 2000 s^{-1} (**Figure 6a**). While the pure vitrimer cannot be processed through the die, all blends produce smooth extrudates and show shear-thinning behaviors with moderate viscosities (below 1000 Pa s for shear rates above 100 s^{-1}). Compared to pure PP (**S0**), at $\dot{\gamma} = 1000$ s^{-1} the viscosities of the blends are increasing in line with the vitrimer fraction, up to 3-fold for **S75**, but remain well within the processing window of a standard extruder. A strong similarity can be found between these results and capillary rheology of conventional TPVs.[58] For all samples the viscosity dependence over shear rate is following a power law decay similarly to highly filled thermoplastics.[26,55,59–61]

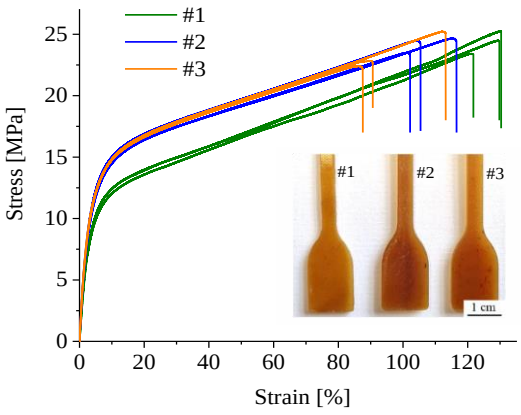

Figure 7. Reprocessing of **S60** by multiple shredding-injection moulding cycles. Tensile tests and corresponding tensile bars, showing first (green solid lines; #1), second (blue solid lines; #2) and third (orange solid lines; #3) reprocessing cycles.

The easy (re)processability of vitrimer blends was further illustrated by injection moulding using sample **S60**. Samples undergoing multiple shredding-injection cycles were analyzed by tensile testing (**Figure 7**), confirming that the mechanical performance remains stable over the number of applied reprocessing cycles. Note that the initial sample (#1) was obtained by hot pressing and shows a modulus of about 2.5 MPa lower than reprocessed samples, in which the PP was oriented during injection. There is no noticeable change of mechanical performance between the second and third reprocessing cycle. Evolution of the percolating vitrimer network over time and during various processes was monitored by repeated stress relaxations at 200 °C.[62] **Figure 8a** shows the relaxation moduli of **S24** immediately after initial synthesis, and upon annealing at 200 °C for several hours in the rheometer.

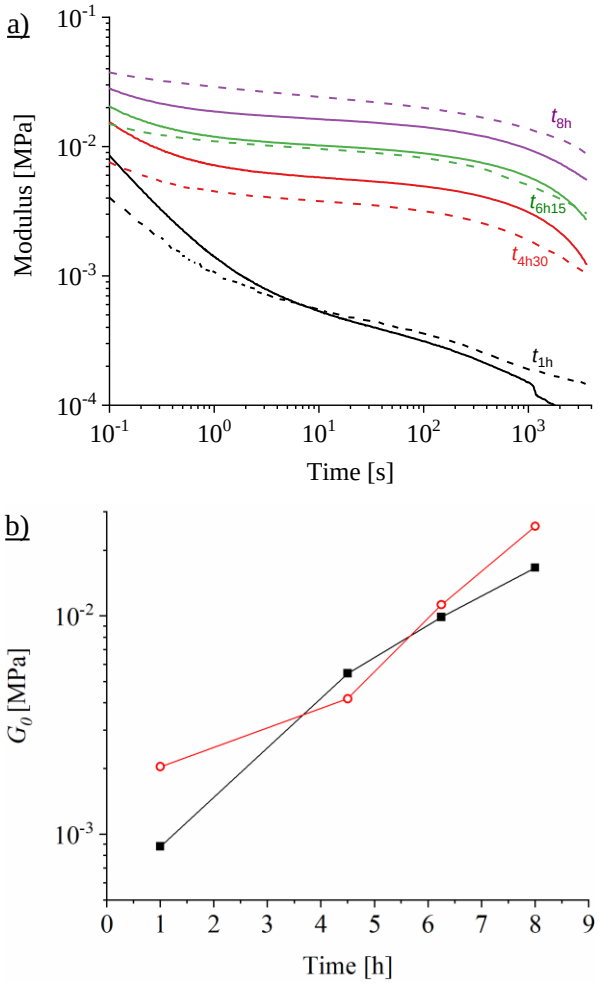

Figure 8. a) Repeated stress relaxations at 200 °C and 1 % strain of **S24** immediately after synthesis (solid lines) and after disrupting the percolating network of annealed **S24** by extrusion at 2000 s^{-1} in the capillary rheometers (dashed lines). Annealing time is given at the end of the experiment, which is 1h (black lines), 4h30 (red lines), 6h15 (green lines) and 8h (purple lines).b) extrapolated G_0 moduli, showing the increase

with time upon annealing from immediately after synthesis (black solid square) and after disrupting the percolating vitrimer network (red open circles).

Initially (*i.e.* after reactive melt blending and pressing), the sample relaxes very fast and does not show any evidence of a percolating network (t_{1h} in **Figure 8a**). The formation of a percolating dynamic network is shown after extended annealing at 200 °C (up to G_N = 17 kPa with a relaxation time of 5400 s). After annealing, **S24** was grinded and extruded at 2000 s^{-1} using the capillary rheometer, initially showing a very low modulus (G_N = 0.6 kPa), demonstrating that high shear considerably alters the vitrimer percolating network. This phenomenon is however reversible, as significant network recovery (G_N = 40 kPa) is obtained after 8h at 200 °C (**Figure 8b**). Similar build-up, break at high shear and recovery of percolating dynamic vitrimer networks are found for other blends. For instance, **S60** immediately after synthesis shows a network modulus G_N about 60 kPa with a relaxation time about 1700 s. The relaxation times quickly evolve to reach a constant value about 5000 s while the modulus continuously increases up to G_N = 130 kPa after 8h at 200 °C (Figure S18a, Supporting Information).

Evidence of the formation of a percolating vitrimer network through annealing is also corroborated by swelling experiments: swelling **S12** immediately after synthesis results in a dispersion of vitrimer particles whereas swelling after annealing for 8h at 200 °C leads to a monolithic piece (Figure S18b, Supporting Information). Dynamic percolation phenomena during static annealing have been observed in the case of polymer nanocomposites, such as PP nanocomposites containing organoclay or nanosilicates.[63–66] Time- and shear-dependent thixotropy or anti-thixotropy (*e.g.* decrease or increase of viscosity with time, respectively) has also been recently observed in silica/polymer nanocomposites featuring dynamic covalent links across interfaces.[67] In TPV, however, this phenomena appears to have been greatly overlooked. In our blends, the dynamics of the percolating vitrimer networks reformation appear to be commensurate with the bond-exchange transesterifications rates determined from stress relaxation experiments. It appears unlikely that this phenomenon would be related to direct coalescence and sintering of vitrimer particles as no evidence of morphological changes can be evidenced upon annealing (Figure S19, Supporting Information), and the phenomenon occurs even in blends containing fractions of vitrimers below the percolation threshold. We believe however that PP-*g*-MA chains grafted on and connecting vitrimer particles via ester bonds might also be involved in dynamic transesterification exchanges and might be the primary cause for the establishment of a dynamic percolating network with yield stress behavior.

3. Conclusion

A facile and up-scalable method for the synthesis of phase-separated vitrimer-thermoplastic blends through reactive mixing has been developed. This process was demonstrated using a well-established epoxy-acid vitrimer system dispersed into a polypropylene matrix. The corresponding blends demonstrate all characteristics of a percolating dynamic network connecting vitrimer domains – with solvent resistance, high-temperature dimensional stability, and stress relaxation. This system has the unique advantage of decoupling exchange dynamics in the vitrimer network from high-shear processing, that occurs through reversible rupture of the percolating vitrimer network and leads to low viscosities with easy processability. This concept addresses a major bottleneck in the current development of vitrimer materials and we believe it will open wide perspectives for high throughput syntheses and processing using conventional tools for thermoplastics such as extrusion, injection moulding, or 3D printing by FDM. Future optimizations of vitrimer-thermoplastic blends are currently ongoing in order to further decrease the size of vitrimer domains, either through processing – using for instance continuous reactive extrusion – or through formulation, such as tuning the amount of compatibilizer. The model strategy system that we present might also be easily generalizable to other combinations of vitrimers (including for instance low T_g or high T_g vitrimer phases) and other thermoplastic phases.

4. Experimental Section/Methods

4.1. Materials

Polypropylene PPH7060 (PP) was obtained from Total Energies. It features a melt flow index of 12 g 10 min^{-1} (at 230 °C, 2.16 kg) and a zero-shear viscosity of 1500 Pa s at 200 °C. HT-SEC in TCB at 150 °C gives M_n = 234 kg $mol^{-1}$and $Đ$ = 5.5. Pripol 1040 (82 wt% trimer, 18 wt% dimer; with an acid value of 185 mg KOH g^{-1}, corresponding a COOH equivalent of 294 g mol_{COOH}^{-1}) with a viscosity of 13 mPa s at 200 °C was supplied by Croda International Plc. Polypropylene grafted maleic anhydride (PP-*g*-MA) Exxelor PO1020 (MA level 1.2 wt%; HT-SEC in TCB at 150 °C: M_n = 36 kg mol^{-1}, $Đ$ = 2.53), with a melt flow index of 430 g 10 min^{-1} (at 230 °C, 2.16 kg) was purchased from ExxonMobil. Irganox1010 was supplied by BASF SE. Aerosil A200 fumed silica (S_{BET} = 225 m^2 g^{-1}, *Ø ca*. 12 nm) was purchased from Evonik Industries. Bisphenol A diglycidyl ether (DGEBA, 98%, Merck), 1,5,7-triazabicyclo[4.4.0]dec-5-ene (TBD, 98%, Merck) and xylene (99%, Acros Organics) were used as received.

4.2. General procedure for the processing of PP/vitrimer blends. Synthesis of S_{60}.

4.2.1 Preparation of Pripol/TBD/silica mixture

TBD (1.18 g, 8.48 mmol, 5 mol% relative to COOH groups of Pripol) was dissolved in Pripol (50.0 g, 170 mmol of COOH groups) by stirring under vacuum at 140 °C in a rotary evaporator. A Hauschild DAC 150.1 FVZ-K SpeedMixer was then used to disperse A200 fumed silica (7.50 g, 15 wt% relative to Pripol) by mixing for 2 min at 3600 rpm.

4.2.2 Synthesis of vitrimer/PP blends by reactive processing

Vitrimer/PP blends were prepared by a stepwise addition of the reactants into an HAAKE Polylab OS RheoDrive 7 internal mixer by ThermoFisher Scientific (volume *ca.* 70 cm^3), operating at 200 °C, 50 rpm, and with a filling level of ca. 40 g. As a representative example for **S_{60}**, a total of 16.0 g dry blend of PP (14.3 g), PP-*g*-MA (1.60 g, 10 wt% relative to the total thermoplastic phase) and Irganox (72 mg, 0.5 wt% relative to PP) were added first. As soon as the torque stabilized (after ca. 5 min), 17.6 g of previously prepared Pripol/TBD/silica mixture were added (containing Pripol (15.0 g, 51.0 mmol of COOH groups), TBD (354 mg, 254 mmol) and 2.25 g of silica), followed by 5 min mixing time, and then the addition of DGEBA (9.00 g, 51.0 mmol of epoxy groups). The reaction was terminated after 10 min. The torque and temperature were monitored throughout the reaction. To prevent cooling and crystallization of PP, the hot blend was transported immediately from the internal mixer inside preheated steel molds to a 200 T hot press. The blends were compressed for 5 min at 200 °C with a stepwise increase of pressure of 50 bar min^{-1}, until 200 bars were reached. The plates were cooled down in the mold at room temperature and the thickness of the produced plates was *ca* 1 mm. This synthesis protocol was applied to blends **S_{12}**, **S_{24}**, **S_{48}** and **S_{75}**. The reference sample **S_0** was produced by mixing 40 g PP and 0.2 g of antioxidant in the same conditions as the blends, for a total mixing time of 20 mins. Immediately after mixing, the samples were pressed in the hot press following the same protocol as the blends. The exact amounts of reagents for each sample are provided in **Table S4**.

*4.2.3 Synthesis of reference sample **S_{100}***

The vitrimer reference **S_{100}** was prepared by mixing 32.9 g of previously prepared Pripol/TBD/silica mixture (containing Pripol (28.1g , 95.6 mmol of COOH groups), TBD (666 mg, 4.78 mmol) and 4.20 g of silica) with DGEBA (16.8 g, 95.6 mmol of epoxy groups) using the speed mixer (total mixing duration of 120 s at 2500 rpm. To avoid overheating during this process and premature curing, 30 s mixing / 2 min cooling cycles were applied). The curing was then done in a 200T hot press at 200 °C. A steel mould

was filled with the unreacted mixture, sandwiched between two steel plates and the pressure increased stepwise by 50 bar min^{-1} until 200 bars were reached. After 15 min, the mould was recovered, and the sample was cooled inside the mould at room temperature.

4.2.4 Reprocessing of PP/vitrimer blends.

The reprocessing of vitrimer blends was done by manually cutting the plates into ca. 1 mm pieces and feeding them into the injection barrel of a Xplore micro injection moulder preheated at 200 °C. After 5 min melting time, the material was compressed and injected into tensile specimen. After tensile testing, the bars were cut and injected again until the desired number of reprocessing steps was reached.

4.4. Characterization Methods

Size exclusion chromatography (SEC): To determine the mollar mass of PP and PP-*g*-MA, SEC was performed using a Malvern Instruments Viscotek system equipped with three columns (Agilent Technologies, PLgel Olexis 300 mm × 7 mm I.D.). A solution (200 µL) was prepared with a concentration of 5 mg mL^{-1} for each sample, which was then eluted in 1,2,4-trichlorobenzene (150 °C, 1 mL min^{-1}). 2,6-di-tert-butyl-4-methylphenol (butylated hydroxytoluene, BHT, 200 mg L^{-1}) was used to stabilize the mobile phase. Detection was performed by using a differential refractive index detector. Number average molar masses (M_n) and chain dispersities ($Đ$) were calculated using calibration curves obtained from poly(ethylene) standards using the OmniSEC 5.02 software.

Fourier-transform infrared spectroscopy (FTIR): The samples were analyzed by a Thermo Scientific Nicolet iS50 FT-IR in transmission mode, with a resolution of 4 cm^{-1} and 32 scans between a wavenumber of 4000 and 600 cm^{-1}. For the analysis ca. 20 µm thick films were pressed with a hot press at 200 °C between Teflon sheets.

Thermogravimetric analysis (TGA): TGA was performed at a heating rate of 10 °C min^{-1} from room temperature to 600 °C, under nitrogen atmosphere using a Mettler Toledo TGA 2 instrument.

Differential scanning calorimetry (DSC): A Mettler Toledo DSC 3^+ device was used to study the samples. Two heating and one cooling ramps at 10 °C min^{-1} were performed between -40 and 200 °C. Only the values of the second cycle were taken.

Dynamic mechanical analysis (DMA): A DMA Q800 device from TA Instruments was used in the tension film mode under a nitrogen atmosphere. Rectangular samples of 1 mm thickness, 5 mm width and approximately 15 mm length were tested at a frequency of 1 Hz and an amplitude of 5 µm. Heating ramps of 3 °C min^{-1} were applied from –80 °C to 220 °C.

Rheological analysis: Rheology measurements were performed using a 25 mm plate-plate geometry with an Ares G2 rotational rheometer from TA Instruments equipped with a convection oven.

Flow curves for Pripol/TBD/silica mixtures were obtained from increasing steps of shear rates (0.001 to 2 s^{-1}), with equilibration times between 30 and 60 s.

Gelation kinetics of the pure vitrimer were monitored by pouring the reactive mixture on the preheated geometries and immediately starting time-resolved small amplitude oscillatory shear (SAOS) experiments at 200 °C.

Samples of vitrimer blends were punched from rectangular plates with a thickness of ca. 1.0 mm, and a diameter of 25 mm, and introduced into the geometries preheated at 200 °C. Frequency sweeps and stress relaxations (SR) were performed with a strain of 1%, within the linear viscoelastic regime of the measured material. The average relaxation time τ* was calculated by fitting relaxation moduli *G*(t) using a stretched exponential decay function:

$$G(t) = G_0 e^{-\left(\frac{t}{\tau_{app}}\right)^{\beta}} \quad (2)$$

where τ_{app} is the apparent relaxation time. The following correction gives τ^*:

$$\tau^* = \frac{\tau_{app}\Gamma\left(\frac{1}{\beta}\right)}{\beta} \quad (3)$$

Successive stress relaxation experiments were performed to study the effect of prolonged annealing on the network properties, by repeating SRs for approximatively 8h.

A Mars 60 Rheometer from ThermoScientific, equipped with a Peltier oven and 8 mm parallel plate geometries was used to perform creep experiments. The stress imposed on the 1 mm thick samples was varied from 50 to 7000 Pa over 600s, at 200 °C.

Capillary rheometry: Experiments were performed in a Malvern Rosand RH10 at 200 °C, using a die with 1 mm diameter, 20 mm length and 180° entrance angle. A 10,000 Psi force captor was used to record the drop of pressure across the capillary. The amount of material required for single-bore measurements is ca. 20 g. We did not carry out Bagley corrections accounting for pressure drop at the entrance of the capillary as they required at least 40 g of materials (dual-bore mode) but specifically chose long capillaries (20 mm) and flat entrance to minimize this issue. Increasing steps of shear rates were applied and the apparent shear stresses τ_{app} were determined from the pressure in front of the capillary after proper equilibration (about 30 s).

The Weißenberg-Rabinowitsch correction was performed automatically. Hence, the corrected shear rate ($\dot{\gamma}_{true}$) was given by:

$$\dot{\gamma}_{true} = \frac{3}{4} \times \dot{\gamma}_{app} + \frac{1}{4} \times \tau_{app} \times \frac{d\,\dot{\gamma}_{app}}{d\,\tau_{app}} \quad (4)$$

where $\dot{\gamma}_{app}$ is the apparent shear rate, and τ_{app} the shear stress, defined by the Hagen/Poiseuille relation for Newtonian fluids. The viscosity was calculated as:

$$\eta = \frac{\tau_{app}}{\dot{\gamma}_{true}} \quad (5)$$

Tensile test: Dumbbell-shaped specimens were analyzed using a Shimadzu AGS-X tensile test machine at ambient temperature equipped with a force sensor of 10 kN and 10 mm min^{-1} crossbar speed. The samples were cut from a plate of 1 mm thickness, with a gauge width and length of 4 mm and 30 mm, respectively. The tensile strength, the elongation at break, and the Young's modulus were calculated for each sample from at least three specimens and the results were averaged. For cyclic tensile tests, injected dumbbell shaped specimen with a thickness of 2 mm, width of 4 mm and 30 mm gauge length were used on a MTS Criterion 42 device. Cyclic testing involves stretching up to ε = 50% and return to initial displacement at 2 mm min^{-1}. A 10 min recovery delay was performed before starting the next cycle.

Optical microscopy (OM): Images were taken on a Leica stereo microscope with a magnification of ×11.7 and ×32.

Scanning Electron Microscopy (SEM): Observations of the sample morphology was done on a FEI Quanta 250 FEG microscope with a voltage of 10 kV using a Secondary Electron detector (SED). For images with enhanced contrast or to identify the different phases, a Backscattered Electron detector (BSE) or an Energy Dispersive X-Ray detector (EDX) was used. The sample surfaces were prepared by cryo-ultramicrotomy using a UCL Leica at −110 °C with an oscillating diamond knife (Diatom), followed by a carbon coating to enhance conductivity.

X-ray analysis: Simultaneous SAXS and WAXS were recorded at the SWING Beamline of SOLEIL Synchrotron source, Saint-Aubin, France. The energy used for all experiments was 12 keV. Samples were melt-pressed into 1 mm thick metal washers, windows on both sides were obtained by sealing Kapton foil with epoxy glue. The samples were inserted in a custom-built heated block and analyzed at 25 and 160 °C. 2D SAXS and WAXS patterns were collected using an EigerX4M detector positioned at 6.5 m from the sample and a Merlin detector, respectively.

Gel Content and swelling ratio were determined by immersing samples (w_0 of ca. 80 mg) in a closed vial in xylene at 110 °C for 48 h. Monolithic, swollen samples were recovered and quickly wiped and weighted (w_S), then dried for 24 h at 40 °C under vacuum (final weight w_d).

The gel content was calculated using the following equation:

$$Gel\ fraction = \frac{W_d}{W_0} \quad (6)$$

The swelling ratio was calculated with the formula:

$$Swelling\ ratio = 1 + \frac{\rho_s \left(\frac{w_s}{w_d} - 1\right)}{\rho_p} \quad (7)$$

where ρ_P and ρ_S are the density of polymer (approximated as 1 g cm^{-3}) and for the solvent (xylene = 0.861 g cm^{-3}), respectively.

Supporting Information

Supporting Information is available from the Wiley Online Library or from the author.

Acknowledgements

We thank the staff of the Technological Centre of Microstructures, Claude Bernard University Lyon 1, especially Pierre Alcouffe, for the support and help conducting the microscopy analyses. We acknowledge SOLEIL for provision of synchrotron radiation facilities and we would like to thank Thomas Bizien for assistance in using beamline SWING. Additionally, we would like to thank François Tournilhac and Diego Cardi (ESPCI, Paris, France) for the fruitful scientific discussions and their support. This project has received funding from the European Union's Horizon 2020 research and innovation programme under the Marie Skłodowska-Curie Grant agreement No 860911 (www.vitrimat.eu).

Conflict of Interest

The authors declare no conflict of interest.

Keywords

vitrimers, thermoplastic vulcanizates, reactive processing, reprocessing, injection molding, thermoplastics, thermosets, viscoelastic properties, rheology

Received: ((will be filled in by the editorial staff))

Revised: ((will be filled in by the editorial staff))

Published online: ((will be filled in by the editorial staff))

[1] J.-P. Pascault, H. Sautereau, J. Verdu, R. J. J. Williams, *Thermosetting Polymers*, CRC Press, **2002**.

[2] D. J. Fortman, J. P. Brutman, G. X. De Hoe, R. L. Snyder, W. R. Dichtel, M. A. Hillmyer, *ACS Sustain. Chem. Eng.* **2018**, *6*, 11145.

[3] C. N. Bowman, C. J. Kloxin, *Angew. Chemie - Int. Ed.* **2012**, *51*, 4272.

[4] G. M. Scheutz, J. J. Lessard, M. B. Sims, B. S. Sumerlin, *J. Am. Chem. Soc.* **2019**, *141*, 16181.

[5] M. Guerre, C. Taplan, J. M. Winne, F. E. Du Prez, *Chem. Sci.* **2020**, *11*, 4855.

[6] J. Zheng, Z. M. Png, S. H. Ng, G. X. Tham, E. Ye, S. S. Goh, X. J. Loh, Z. Li, *Mater. Today* **2021**, *51*, 586.

[7] A. Jourdain, R. Asbai, O. Anaya, M. M. Chehimi, E. Drockenmuller, D. Montarnal, *Macromolecules* **2020**, *53*, 1884.

[8] M. M. Obadia, A. Jourdain, P. Cassagnau, D. Montarnal, E. Drockenmuller, *Adv. Funct. Mater.* **2017**, *27*, 1703258.

[9] B. R. Elling, W. R. Dichtel, *ACS Cent. Sci.* **2020**, *6*, 1488.

[10] T. Shen, Z. Song, S. Cai, F. J. Vernerey, *Proc. Natl. Acad. Sci. U. S. A.* **2021**, *118*.

[11] N. H. Cho, B. M. El-zaatari, R. Gokarn, S. Wang, S. L. Craig, A. Kalow, Julia, J. J. Richards, *ChemRxiv* **2023**. https://doi.org/10.26434/chemrxiv-2023-hb4v1

[12] L. Yu, X. Sun, Y. Jin, W. Zhang, R. Long, *Int. J. Mech. Sci.* **2021**, *201*, 106466.

[13] Q. Shi, C. Jin, Z. Chen, L. An, T. Wang, *Adv. Funct. Mater.* **2023**.

[14] F. Meng, M. O. Saed, E. M. Terentjev, *Nat. Commun.* **2022**, *13*.

[15] X. Cui, N. Jiang, J. Shao, H. Zhang, Y. Yang, P. Tang, *Macromolecules* **2022**.

[16] R. G. Ricarte, F. Tournilhac, M. Cloître, L. Leibler, *Macromolecules* **2020**, *53*, 1852.

[17] M. Rottger, T. Domenech, R. van der Weegen, A. Breuillac, R. Nicolay, L. Leibler, *Science* **2017**, *65*, 62.

[18] J. Tellers, R. Pinalli, M. Soliman, J. Vachon, E. Dalcanale, *Polym. Chem.* **2019**, *10*, 5534.

[19] M. Maaz, A. Riba-Bremerch, C. Guibert, N. J. Van Zee, R. Nicolaÿ, *Macromolecules* **2021**, *54*, 2213.

[20] C. Taplan, M. Guerre, J. M. Winne, F. E. Du Prez, *Mater. Horizons* **2020**, *7*, 104.

[21] X. Xu, S. Ma, H. Feng, J. Qiu, S. Wang, Z. Yu, J. Zhu, *Polym. Chem.* **2021**, *12*, 5217.

[22] S. Yu, F. Li, S. Fang, X. Yin, S. Wu, Z. Tang, L. Zhang, B. Guo, *Macromolecules* **2022**, *55*, 3236.

[23] A. Y. Coran, R. Patel, *Rubber-Thermoplastic Compositions. Part Viii. Nitrile Rubber Polyolefin*

Blends With Technological Compatibilization., Vol. 56, **1983**, pp. 1045–1060.

[24] A. V. MacHado, M. Van Duin, *Polymer* **2005**, *46*, 6575.

[25] F. Goharpey, A. A. Katbab, H. Nazockdast, *J. Appl. Polym. Sci.* **2001**, *81*, 2531.

[26] R. Rajesh Babu, N. K. Singha, K. Naskar, *Polym. Eng. Sci.* **2010**, *50*, 455.

[27] H. Wu, M. Tian, L. Zhang, H. Tian, Y. Wu, N. Ning, *Soft Matter* **2014**, *10*, 1816.

[28] C. Le Hel, V. Bounor-Legaré, M. Catherin, A. Lucas, A. Thèvenon, P. Cassagnau, *Polymers* **2020**, *12*, 1.

[29] H. Wu, M. Tian, L. Zhang, H. Tian, Y. Wu, N. Ning, T. W. Chan, *ACS Sustain. Chem. Eng.* **2015**, *3*, 26.

[30] S. Li, H. Tian, B. Zhang, G. H. Hu, C. Y. Liu, L. Zhang, M. Tian, *Polymer* **2019**, *181*.

[31] D. Montarnal, M. Capelot, F. Tournilhac, L. Leibler, *Science* **2011**, *334*, 965.

[32] C. Ye, V. S. D. Voet, R. Folkersma, K. Loos, *Adv. Mater.* **2021**, *33*, 1.

[33] Q. Shi, K. Yu, X. Kuang, X. Mu, C. K. Dunn, M. L. Dunn, T. Wang, H. Jerry Qi, *Mater. Horizons* **2017**, *4*, 598.

[34] E. Chabert, J. Vial, J. P. Cauchois, M. Mihaluta, F. Tournilhac, *Soft Matter* **2016**, *12*, 4838.

[35] F. I. Altuna, V. Pettarin, R. J. J. Williams, *Green Chem.* **2013**, *15*, 3360.

[36] C. Bakkali-Hassani, P. Edera, J. Langenbach, Q. A. Poutrel, S. Norvez, M. Gresil, F. Tournilhac, *ACS Macro Lett.* **2023**, 338.

[37] M. Capelot, M. M. Unterlass, F. Tournilhac, L. Leibler, *ACS Macro Lett.* **2012**, *1*, 789.

[38] Y. Zhou, J. G. P. Goossens, R. P. Sijbesma, J. P. A. Heuts, *Macromolecules* **2017**, *50*, 6742.

[39] T. N. Tran, E. Rawstron, E. Bourgeat-Lami, D. Montarnal, *ACS Macro Lett.* **2018**, *7*, 376.

[40] H. Pernot, M. Baumert, F. Court, L. Leibler, *Nat. Mater.* **2002**, *1*, 54.

[41] D. B. Todd, In *Handbook of Industrial Mixing*, John Wiley & Sons, Inc., Hoboken, NJ, USA, **2004**, pp. 987–1025.

[42] L. A. Utracki, H. Shi, *Polym. Eng. Sci.* **1992**, *32*, 1824.

[43] R. W. Flumerfeltl, *Ind. Eng. Chem. Fundam.* **1972**, *11*.

[44] G. Martin, C. Barres, P. Sonntag, N. Garois, P. Cassagnau, *Eur. Polym. J.* **2009**, *45*, 3257.

[45] P. Pötschke, D. R. Paul, *J. Macromol. Sci. - Polym. Rev.* **2003**, *43*, 87.

[46] G. Guerra, V. Petraccone, P. Corradini, C. De Rosa, R. Napolitano, B. Pirozzi, G. Giunchi, *J. Polym. Sci. Part A-2, Polym. Phys.* **1984**, *22*, 1029.

[47] S. Brückner, S. V. Meille, V. Petraccone, B. Pirozzi, *Prog. Polym. Sci.* **1991**, *16*, 361.

[48] T. Inoue, T. Suzuki, *J. Appl. Polym. Sci.* **1996**, *59*, 1443.

[49] R. M. A. l'Abee, M. van Duin, A. B. Spoelstra, J. G. P. Goossens, *Soft Matter* **2010**, *6*, 1758.

[50] H. Wu, M. Tian, L. Zhang, H. Tian, Y. Wu, N. Ning, G.-H. Hu, *Polymers* **2016**, *8*, 127.

[51] A. Legrand, C. Soulié-Ziakovic, *Macromolecules* **2016**, *49*, 5893.

[52] Z. Yang, Q. Wang, T. Wang, *ACS Appl. Mater. Interfaces* **2016**, *8*, 21691.

[53] Y. Yang, Z. Pei, X. Zhang, L. Tao, Y. Wei, Y. Ji, *Chem. Sci.* **2014**, *5*, 3486.

[54] N. G. McCrum, B. E. Read, G. William, *Anelastic and dielectric effects in polymeric solids*, John Wiley & Sons, NY, **1967**.

[55] N. Ghahramani, K. A. Iyer, A. K. Doufas, S. G. Hatzikiriakos, *J. Rheol.* **2020**, *64*, 1325.

[56] D. Bourry, B. D. Favis, *J. Polym. Sci. Part B Polym. Phys.* **1998**, *36*, 1889.

[57] T. S. Omonov, C. Harrats, P. Moldenaers, G. Groeninckx, *Polymer* **2007**, *48*, 5917.

[58] I. A. Goettlier, J. R. Richwine, J. Wille, *Rubber Chem. Technol.* **1982**, *55*, 1448.

[59] S. Saha, A. K. Bhowmick, **2020**, *48758*, 1.

[60] W. G. F. Sengers, P. Sengupta, J. W. M. Noordermeer, S. J. Picken, A. D. Gotsis, *Polymer* **2004**, *45*, 8881.

[61] A. Zohrevand, F. Goharpey, J. Nasrollah Gavgani, R. Foudazi, *Polym. Compos.* **2020**, *41*, 1376.

[62] D. Z. Khedaioui, C. Tribout, J. Bratasanu, F. D'Agosto, C. Boisson, D. Montarnal, *Angew. Chemie Int. Ed.* **2023**, *62*.

[63] R. Zouari, T. Domenech, B. Vergnes, E. Peuvrel-Disdier, *J. Rheol.* **2012**, *56*, 725.

[64] P. Reichert, B. Hoffmann, T. Bock, R. Thomann, R. Mülhaupt, C. Friedrich, *Macromol. Rapid Commun.* **2001**, *22*, 519.

[65] M. Rueda, R. Fulchiron, P. Cassagnau, A. Prebé, G. Martin, *J. Rheol.* **2016**, *60*, 1245.

[66] P. Cassagnau, F. Mélis, *Polymer* **2003**, *44*, 6607.

[67] G. L. Jackson, J. M. Dennis, N. D. Dolinski, M. Van Der Naald, H. Kim, C. Eom, S. J. Rowan, H. M. Jaeger, *Macromolecules* **2022**, *55*, 6453.